Published in final edited form as:
Phys Med Biol. 2013 January 21; 58(2): . doi:10.1088/0031-9155/58/2/261.

Quenching correction for volumetric scintillation dosimetry of proton beams

Daniel Robertson[1,2], **Dragan Mirkovic**[1,2], **Narayan Sahoo**[1,2], and **Sam Beddar**[1,2]

[1]Department of Radiation Physics, The University of Texas MD Anderson Cancer Center, Houston, Texas 77030

[2]The University of Texas Graduate School of Biomedical Sciences at Houston, Houston, Texas 77030

Abstract

Purpose—Volumetric scintillation dosimetry has the potential to provide fast, high-resolution, three-dimensional radiation dosimetry. However, scintillators exhibit a nonlinear response at the high linear energy transfer (LET) values characteristic of proton Bragg peaks. The purpose of this study was to develop a quenching correction method for volumetric scintillation dosimetry of proton beams.

Methods—Scintillation light from a miniature liquid scintillator detector was measured along the central axis of a 161.6-MeV proton pencil beam. Three-dimensional dose and LET distributions were calculated for 85.6-, 100.9-, 144.9-, and 161.6-MeV beams using a validated Monte Carlo model. LET values were also calculated using an analytical formula. A least-squares fit to the data established the empirical parameters of a quenching correction model. The light distribution in a tank of liquid scintillator was measured with a CCD camera at all four beam energies. The quenching model and LET data were used to correct the measured light distribution.

Results—The calculated and measured Bragg peak heights agreed within ±3% for all energies except 85.6 MeV, where the agreement was within ±10%. The quality of the quenching correction was poorer for sharp low-energy Bragg peaks because of blurring and detector size effects. The corrections performed using analytical LET values resulted in doses within 1% of those obtained using Monte Carlo LET values.

Conclusion—The proposed method can correct for quenching with sufficient accuracy for dosimetric purposes. The required LET values may be computed effectively using Monte Carlo or analytical methods. Future detectors should improve blurring correction methods and optimize the pixel size to improve accuracy for low-energy Bragg peaks.

1. Introduction

Volumetric scintillation dosimetry is a promising new area of study with the goal of making fast, high-resolution measurements of three-dimensional (3D) dose distributions. Interest in 3D dosimetry has increased as highly modulated conformal radiation therapy techniques have grown more complex and become common in the clinic. The 3D dosimetry approach is particularly important for proton therapy because the finite range of the proton beam makes it possible to modulate the dose in depth. As a result, it is not possible to predict the proton beam dose at all depths on the basis of the dose at a single depth, as is the case with photon-based modalities. Therefore, measurements must be made at multiple depths to fully

abeddar@mdanderson.org.

characterize a proton beam dose distribution (ICRU, 2007). For instance, the clinical standard for patient-specific quality assurance at the Proton Therapy Center–Houston is to measure intensity-modulated proton therapy treatment fields by delivering each field multiple times to a two-dimensional array of ionization chambers placed at different depths in a plastic water phantom (Arjomandy *et al.*, 2010). The quality assurance process can take 6-8 hours per patient, limiting the number of patients who can benefit from intensity-modulated proton therapy.

Three-dimensional scintillation dosimetry with a liquid scintillator (LS) was originally proposed and explored by Kirov et al. (2000; 2005) for brachytherapy eye plaques in a small detection volume. Fukushima et al. subsequently developed a proton beam range-measurement tool using a long, narrow block of plastic scintillator (2006). Our research group has developed a large-volume LS detector with the goal of rapidly measuring 3D dose distributions (Beddar *et al.*, 2009; Ponisch *et al.*, 2009; Archambault *et al.*, 2012). This detector system exhibits a linear dose response, a spatial resolution of 0.3 mm, and a temporal resolution of 0.05 seconds (Archambault *et al.*, 2012). The current system gathers light from a single viewing angle. However, future detectors will measure from multiple viewing angles, making 3D dose reconstruction possible. The functional principle behind volumetric scintillation dosimetry is the gathering of light emissions from a volume of scintillating material, followed by 3D reconstruction of the light distribution. If the light emission from the scintillator is proportional to the dose deposition, then the measured light distribution is equivalent to a relative dose distribution. This process is complicated in proton beams by a phenomenon known as ionization quenching. While the mechanism of ionization quenching is not fully understood, the result is an underresponse of the scintillator in regions with a very high ionization density (Birks, 1951; Chou, 1952). This condition is met in the Bragg peak of therapeutic proton beams, where the low proton energy corresponds to a sharp increase in the stopping power (ICRU, 1993). Ionization quenching removes the linear relationship between dose and scintillation light in proton beams, making scintillation dosimetry for proton beams more challenging.

The goal of this study was to develop an ionization quenching correction method to restore the linear dose response of scintillators irradiated by proton beams. The quenching correction method is based on an empirical model that predicts quenching on the basis of the linear energy transfer (LET) of the proton beam (Birks, 1951). A recent study found that this model can be used to correct for quenching in plastic scintillator detectors, showing an agreement within 5% between scintillator and ionization chamber measurements of proton beams (Wang *et al.*, 2012).

The LET values were calculated using Monte Carlo and analytical methods. The material-specific quenching coefficient for the scintillator was obtained by measuring the light emission as a function of depth using a novel miniature liquid scintillator detector. This approach ensured that the measured quenching coefficient was independent of optical artefact corrections associated with the volumetric detector. The quenching correction method was applied to images from the volumetric detector, and the accuracy of the corrected dose measurements was determined by comparing them with doses calculated using a validated Monte Carlo model.

2. Materials and methods

2.1. Quenching model

In this study, ionization quenching was modelled using the empirical formula developed by Birks (1951). This model describes scintillation light emission in terms of the stopping power of the scintillator for the particle beam:

$$dS/dx = \frac{A \cdot dE/dx}{1 + kB \cdot dE/dx} \quad (1)$$

where S is the scintillation light emitted, dE/dx is the energy deposited by the protons over a distance x in the medium, A is the scintillation efficiency of the medium, and k and B are empirical factors describing the nonscintillation energy loss in the medium. An additional multiplicative factor ε should technically be added to account for the collection efficiency of the light, which is dependent on the detector geometry and the attenuating properties of the materials. However, in this work ε is implicitly included in the parameter A. In the Birks model, $B \cdot dE/dx$ is the specific density of ionized and excited molecules along the particle track, and k is the quenching parameter (Birks, 1964). These two values are difficult to obtain individually from measurements, so as a general practice k and B are treated together as a single parameter kB.

When a realistic therapeutic proton beam is considered, it is appropriate to replace the stopping power term of the Birks equation with LET, which is defined as the average stopping power in a given region (Berger, 1993; ICRU, 1970). LET values can be generated via Monte Carlo calculations or using an analytical equation, such as that developed by Wilkens and Oelfke (2002). While the analytical method allows for arbitrarily small values of dx, the use of Monte Carlo calculations requires a finite voxel size. Measurements of scintillation light also require a finite detection volume. We can rewrite equation 1 in terms of finite voxels as follows:

$$S_v = \frac{A \cdot L_v}{1 + kB \cdot L_v} \phi_v \quad (2)$$

where S_v is the light emitted from a voxel of volume v, L_v is the track-averaged LET within the voxel, and φ_v is the particle fluence in the voxel. The track-averaged LET is defined as the arithmetic mean of the stopping power of all protons in a given region. Because L_v is an average LET value, it does not provide information about the absolute energy deposited in the voxel. The fluence term (φ_v) is added to scale the emitted light according to the energy deposited.

2.2. Quenching correction factors

To convert a LS detector's light signal into a dose measurement, a quenching correction factor is required. This factor may take the form

$$Q_v = \frac{E_v}{S_v} \quad (3)$$

where Q_v, the correction factor for voxel v, is the ratio of the deposited energy to the emitted light for voxel v. In this form, the energy deposited in a voxel can be recovered by multiplying the correction factor by the light emitted from a voxel. Because the energy deposited in a voxel is equivalent to the track-averaged LET in that voxel multiplied by the particle fluence through the voxel,

$$E_v = L_{t,v} \cdot \phi_v \quad (4)$$

we can combine equations 2, 3, and 4 to describe the quenching correction factor as

$$Q_v = \frac{1 + kB \cdot L_v}{A}. \quad (5)$$

In our prototype, each pixel in the charge-coupled device (CCD) camera measures the light emitted from a column of LS extending from the window to the back of the tank. The column corresponding to each pixel is treated as a single voxel, with the dose and LET averaged over the entire column. By applying the quenching correction factors to all pixels, one obtains a two-dimensional projection of the dose distribution in the LS tank. This distribution can be compared to dose projections from a treatment planning system or Monte Carlo calculation.

2.3. LS detector system

The LS detector system has been described in previous publications (Ponisch *et al.*, 2009; Beddar *et al.*, 2009). It consists of a tank of LS with dimensions of 20×20×23 cm^3. The LS (BC-531, Saint Gobain) consists of fluorescing molecules in a linear alkyl benzene solvent with a physical density of 0.87 g/cm^3 as given by the manufacturer and a measured water equivalent thickness of 0.872 cm. The LS emits photons with a wavelength distribution centred at 425 nm. The tank is constructed of opaque gray polyvinyl chloride (PVC) with a clear polymethyl methacrylate (PMMA) viewing window on one side. The PVC continues past the viewing window, forming a light-tight housing 70 cm beyond the tank, for a total length of 90 cm (figure 1). A CCD camera (Andor Luca S) is attached to the far end and fit with an objective lens to bring the LS volume into focus. The CCD has a resolution of 658×496 pixels, and the effective pixel size at the centre of the tank is 0.29 mm.

2.4. Image processing

The CCD images were processed to correct for artefacts introduced by the camera and the detector geometry. Background subtraction was performed using the average of a sequence of dark images. Depending on the timing of the camera acquisition and the number of monitor units delivered, consecutive images were needed to measure the entire beam delivery. In these cases, the images were summed to provide the total light measurement. A spatial median filter was used to remove random spikes caused by stray radiation incident on the CCD chip, as demonstrated previously (Archambault *et al.*, 2008). A lens calibration technique developed by the computer vision community was used to correct for lens aberrations (Bouguet, 2010). Vignetting was corrected by assuming a cos4q vignetting function, and refraction at the tank-air interface was accounted for by calibrating the pixel size with a grid inside the LS tank. Blurring caused by light scatter in the LS was corrected by deconvolving a mathematically modelled point spread function from each image.

2.5. Monte Carlo LET and dose data

Three-dimensional LET and dose distributions of proton pencil beams were calculated using the Monte Carlo radiation transport code MCNPX, version 2.7d (Waters *et al.*, 2002). These data were calculated for 85.6-, 100.9-, 144.9-, and 161.6-MeV proton beams using validated phase space models of the scanning beam nozzle at the Proton Therapy Center–Houston. The phase space files were generated from a complete model of the nozzle based on blueprints and validated with dose measurements (Sawakuchi *et al.*, 2010). The geometry of the Monte Carlo model mimicked the experimental setup, with the proton beam perpendicularly incident on the face of a cubic phantom of water or LS. The face of the phantom was located at the gantry isocenter. The tallies were counted on a cubic grid measuring 8×8 cm^2 perpendicular to the beam and extending 1 cm or more beyond the end of the Bragg peak for each energy. The voxel size was 1×1 mm^2 perpendicular to the beam,

and the length of the voxels in the beam direction was 1 mm in the proximal build-up region and 0.1 mm in the Bragg peak.

For each beam energy, 5×10^7 incident protons were simulated, resulting in an uncertainty of less than 1% for all voxels with doses exceeding 2% of the maximum dose. All secondary particles were tracked. The energy deposition and particle flux and their uncertainties were scored in each voxel. The track-averaged LET was used in this study for simplicity and was calculated by dividing the energy deposition in each voxel by the particle fluence. The same equations and quenching correction method could be used with the dose-averaged LET if desired, but the values of the empirical parameters would change.

2.6. Analytical LET calculation

While the quenching parameters in this study were primarily determined using LET values calculated with the Monte Carlo model, LET values were also calculated using an analytical formula for comparison. Analytical LET calculation methods are much faster than Monte Carlo methods, and speed is an important consideration in situations involving numerous beam energies or complex geometries. The analytical method of Wilkens and Oelfke (2002) was used to calculate LET values on the central axis of the beam. For 3D calculations, this model assumes a laterally constant LET (Wilkens and Oelfke, 2004). This approximation is justified by the small magnitude of the off-axis changes in LET.

2.7. Quenching parameter determination

The empirical parameters of the Birks model were determined by fitting the model to match measured light emissions and calculated LET values. To decouple the Birks parameters from the optical artefact corrections that were applied to the CCD images, an alternate means of scintillation light measurement was employed to determine the Birks parameters. Miniature LS detectors were constructed using optical fibres. The optical fibres consisted of a 1-mm-diameter clear plastic core covered by a 0.6-mm-thick opaque cladding, for a total diameter of 2.2 mm. A section of cladding was removed, and one end of the cladding was sealed to form a cap. This cap was filled with LS and glued to a section of stripped fibre (figure 2). The resulting assembly consisted of a cylinder of LS with a diameter of 1 mm and a length of 5 mm (for a total volume of approximately 0.004 cm^3) in direct contact with the optical fibre. The fibre ends were inserted into a modified lens cover connected to the CCD camera lens, allowing the camera to measure the light output from several miniature detectors simultaneously.

The linearity of the miniature LS detector response was verified using a clinical 6-MV photon beam (Varian 6EX). Several miniature detectors were placed in an acrylic phantom and irradiated with a 10×10-cm^2 field with exposures ranging from 50 to 500 monitor units. To account for the presence of Cerenkov light produced in the LS and fibres, a fibre with no detector was irradiated simultaneously, and the signal from this fibre was subtracted from the signal in the detectors, following the method proposed by Beddar *et. al.*(1992a, b). Cerenkov light is minimal in proton beams in the therapeutic energy range, so this subtraction is unnecessary for proton beam measurements.

Two miniature LS detectors and one fibre with no detector were used to measure the light signal on the central axis of a 161.6-MeV proton pencil beam in the scanning beam gantry at the Proton Therapy Center–Houston. The measurements were performed in a water-equivalent plastic phantom using a constant source-to-surface distance. For each measurement, 20 monitor units were delivered (as defined by Gillin et al. (2010)), and the light signal was measured by the CCD camera in a single exposure. The depth was corrected according to the measured water equivalent thickness of the plastic slabs.

The quenching correction factors were calculated using equation 5 with LET values generated by the Monte Carlo calculations described in section 2.5. These correction factors were applied to the light signal from the miniature LS detectors. The difference between the corrected scintillation signal and the Monte Carlo central-axis dose was then minimized using a least-squares curve-fitting algorithm to determine the optimal values of A and kB. An additional scaling factor was folded into the parameter A to account for differences in the light collection geometry between the miniature LS detectors and the large-volume LS detector system.

2.8. Quenching correction

To test the effectiveness of the quenching correction method, scintillation light distributions were measured with the large-volume LS detector for pencil beams with energies of 85.6, 100.9, 144.9, and 161.6 MeV. Quenching correction factors were calculated for each CCD pixel by applying equation 5 with the optimized quenching parameters from the miniature LS detector experiment. One set of correction factors was generated using LET values from the Monte Carlo calculations, and another was generated using LET values from the analytical method. Projected dose distributions for the four pencil beams were obtained by multiplying the light distributions by the correction factors.

The corrected light measurements from the LS detector system were compared to projected dose distributions from Monte Carlo calculations for the four beam energies. The degree of agreement was evaluated qualitatively by comparing depth-dose profiles on the beam axis and cross-plane profiles at three depths corresponding to the proximal build-up region (3.5 cm depth), the proximal 50% dose, and the centre of the Bragg peak for each beam energy. The degree of agreement was evaluated quantitatively by comparing the peak-to-plateau ratio and the Bragg peak height for the calculated dose, the measured light signal, and the corrected signal. The peak-to-plateau ratio was defined as the ratio of the dose or signal at the centre of the Bragg peak to the dose or signal at 3.5 cm depth on the beam's central axis.

3. Results

3.1. Miniature LS detector linearity

The LS detectors showed excellent linearity in their dose response. Because the linearity test was performed in a 6-MV photon beam, the scintillation light was mixed with Cerenkov light. After subtraction of the Cerenkov contribution, a linear fit of scintillation light versus the monitor units delivered by the linear accelerator exhibited an R^2 value of 0.9999 (figure 3), indicating excellent linearity. No Cerenkov light was detected when the LS was irradiated in proton beams.

3.2. LET calculation

The Monte Carlo and analytical LET values agreed within ±5% on the central axis of the proton beam (figure 4). The maximum quenching correction factor calculated in this study was 25%, which translates to a maximum dose error of 1.25% when using analytical LET values. In practice, the corrected dose using analytical LET values differed by less than 1% from the corrected dose using Monte Carlo LET values, because the analytical LET equation was more accurate in the Bragg peak region where the largest quenching correction factors occurred. This level of error is comparable to the noise level of the CCD chip and does not significantly affect dose measurements. The off-axis LET values differed by as much as 22% in pixels containing 1% or more of the peak dose (figure 5). This increase occurred mainly in very low dose regions, and it did not result in an appreciable effect on the corrected dose (figure 6).

3.3. Quenching parameter determination

The correction factors produced by equation 5 with the optimized Birks parameters resulted in very close agreement between the corrected light signal and the calculated dose distribution (figure 7). The empirical parameters from this fit were as follows: $A = 1.94\times10^5$, $kB = 9.22$ mg cm^{-2} MeV^{-1}. The parameter A is a scaling factor that is dependent on the detector geometry and the number of particles in the Monte Carlo calculation, but kB is characteristic of the scintillating material and should not change with the experimental setup. The measured value of kB is similar to the measured kB values of other organic scintillators, which vary from 6.6 to 10.4 mg cm^{-2} MeV^{-1} (Birks, 1964).

3.4. Quenching correction

The corrected CCD measurements agreed closely with the Monte Carlo dose calculations as shown in figures 6, 8, and 9. The peak-to-plateau ratios for the calculated doses and corrected scintillation signals agreed well, while the peak-to-plateau ratios for the uncorrected scintillation signals were significantly decreased (table 1). The calculated and measured Bragg peak heights agreed within 3% for all energies except 85.6 MeV, for which the agreement was within 10% (table 2). The lateral penumbrae of the corrected light signals were slightly wider than the penumbrae of the calculated doses (figure 10). The greatest dose errors were found in the steep dose gradients in the Bragg peak, reaching 5% error in the proximal side of the Bragg peak and significantly higher in the distal Bragg peak. The dose in these regions is particularly sensitive to the alignment of the Monte Carlo and CCD data sets as well as the parameters of the deblurring algorithm and detector size effects in the CCD and Monte Carlo verification measurements. While the dose difference was significant in these regions, the distance to agreement was less than 1 mm.

4. Discussion

The primary source of uncertainty in this study is the steep dose gradients and narrow high-dose regions present in proton Bragg peaks. This source of error was present throughout the measurements, including the determination of the scintillator's kB factor with the miniature detectors. The accuracy of the kB factor measurement may be increased by repeating the experiment with a more slowly-varying dose and LET distribution, such as a proton or carbon ion spread-out Bragg peak.

The decision to use Monte Carlo dose calculations as the standard of comparison in this study was appropriate considering the high resolution made possible by Monte Carlo and because of the availability of a carefully validated Monte Carlo model of the PTCH beamline. However, uncertainties in the measurements used to validate the Monte Carlo model may contribute to the differences between the calculated doses and those measured with the LS detector.

The quenching correction method proved to be effective for higher proton beam energies and less effective for the lowest energies. This decreased agreement is due to the increased sharpness of the proton Bragg peak at low energies. Measurements of very sharp Bragg peaks are prone to detector size effects. The thickness of the Monte Carlo voxels in the beam direction was set at 0.1 mm in the Bragg peak region in an attempt to avoid detector size effects. However, the effective pixel size of the CCD camera is 0.3 mm. While this may seem small, it is not small compared to the width of the Bragg peak for an 85.6-MeV proton beam, which is approximately 2 mm full width at half maximum. The result is a broader peak in the light measurement.

Additional difficulties with the very sharp low-energy peaks include imperfections in the deblurring process and imperfect alignment between the calculated and measured data. The observed difficulties with quenching correction at low energies are likely due to a combination of these effects. These effects may also be responsible for the wider lateral penumbrae of the corrected light signals. Future volumetric scintillation dosimetry systems should be optimized to obtain the smallest possible pixel size while still maintaining adequate signal collection. The current system may be further optimized by a detailed study of the point spread function of the camera system, which would facilitate improvements in the deblurring process.

5. Conclusion

We have developed a method to correct for scintillation quenching in a large detection volume with sufficient accuracy to fulfil dosimetric quality assurance and verification purposes. This method requires prior knowledge of the LET distribution of the beam and the Birks model parameters for the scintillator. We have calculated the LET distribution using Monte Carlo and analytical methods and measured the Birks parameters for the liquid scintillator BC-531. Our results suggest that analytical LET calculation methods are adequate for determining the required LET distributions. This study demonstrates the effectiveness of a correction method that restores the linear dose response of a liquid scintillator throughout the proton beam range. The correction method is applied to a large-volume scintillation detector, addressing a major obstacle to fast 3D dosimetry of proton beams.

Acknowledgments

We would like to thank Dr. Uwe Titt for his assistance in interpreting the results of our Monte Carlo calculations and for providing access to the phase space files for the Proton Therapy Center–Houston scanning beam gantry. The project described was supported by award number P01CA021239 from the National Cancer Institute. The content is solely the responsibility of the authors and does not necessarily represent the official views of the National Cancer Institute or the National Institutes of Health. This research was performed in partial fulfillment of the requirements for the Ph.D. degree from The University of Texas Graduate School of Biomedical Sciences at Houston.

References

Archambault L, Briere TM, Beddar S. Transient noise characterization and filtration in CCD cameras exposed to stray radiation from a medical linear accelerator. Med. Phys. 2008; 35:4342–4351. [PubMed: 18975680]

Archambault L, Poenisch F, Sahoo N, Robertson D, Lee A, Gillin MT, Mohan R, Beddar S. Verification of proton range, position, and intensity in IMPT with a 3D liquid scintillator detector system. Med. Phys. 2012; 39:1239–1246. [PubMed: 22380355]

Arjomandy B, Sahoo N, Ciangaru G, Zhu R, Song X, Gillin M. Verification of patient-specific dose distributions in proton therapy using a commercial twodimensional ion chamber array. Med. Phys. 2010; 37:5831–5837. [PubMed: 21158295]

Beddar AS, Mackie TR, Attix FH. Cerenkov Light Generated in Optical Fibers and Other Light Pipes Irradiated by Electron-Beams. Phys. Med. Biol. 1992a; 37:925–935.

Beddar AS, Mackie TR, Attix FH. Water-Equivalent Plastic Scintillation Detectors for High-Energy Beam Dosimetry .1. Physical Characteristics and Theoretical Considerations. Phys. Med. Biol. 1992b; 37:1883–1900. [PubMed: 1438554]

Beddar S, Archambault L, Sahoo N, Poenisch F, Chen GT, Gillin MT, Mohan R. Exploration of the potential of liquid scintillators for real-time 3D dosimetry of intensity modulated proton beams. Med. Phys. 2009; 36:1736–1743. [PubMed: 19544791]

Berger, MJ. NIST Interagency/Internal Report,. Gaithersburg, MD: National Institute of Standard and Technology; 1993. Penetration of proton beams through water I. Depth-dose distribution, spectra, and LET distribution.

Birks JB. Scintillations from Organic Crystals: Specific Fluorescence and Relative Response to Different Radiations. Proceedings of the Physical Society. Section A. 1951; 64:874.

Birks, JB. The Theory and Practice of Scintillation Counting. Oxford, England: Pergamon Press; 1964.

Bouguet J-Y. Camera Calibration Toolbox for Matlab. 2010

Chou CN. The Nature of the Saturation Effect of Fluorescent Scintillators. Physical Review. 1952; 87:904.

Fukushima Y, Hamada M, Nishio T, Maruyama K. Development of an easy-to- handle range measurement tool using a plastic scintillator for proton beam therapy. Phys. Med. Biol. 2006; 51:5927–5936. [PubMed: 17068374]

Gillin MT, Sahoo N, Bues M, Ciangaru G, Sawakuchi G, Poenisch F, Arjomandy B, Martin C, Titt U, Suzuki K, Smith AR, Zhu XR. Commissioning of the discrete spot scanning proton beam delivery system at the University of Texas MD Anderson Cancer Center, Proton Therapy Center, Houston. Med. Phys. 2010; 37:154–163. [PubMed: 20175477]

ICRU. Report 16: Linear energy transfer. Journal of the ICRU. 1970

ICRU. Report 49: Stopping powers and ranges for protons and alpha particles. Journal of the ICRU. 1993

ICRU. Report 78: Prescribing, recording, and reporting proton-beam therapy. Journal of the ICRU 7. 2007

Kirov AS, Piao JZ, Mathur NK, Miller TR, Devic S, Trichter S, Zaider M, Soares CG, LoSasso T. The three-dimensional scintillation dosimetry method: test for a Ru-106 eye plaque applicator. Phys. Med. Biol. 2005; 50:3063–3081. [PubMed: 15972981]

Kirov AS, Shrinivas S, Hurlbut C, Dempsey JF, Binns WR, Poblete JL. New water equivalent liquid scintillation solutions for 3D dosimetry. Med. Phys. 2000; 27:1156–1164. [PubMed: 10841423]

Ponisch F, Archambault L, Briere TM, Sahoo N, Mohan R, Beddar S, Gillin MT. Liquid scintillator for 2D dosimetry for high-energy photon beams. Med. Phys. 2009; 36:1478–1485. [PubMed: 19544763]

Sawakuchi GO, Mirkovic D, Perles LA, Sahoo N, Zhu XR, Ciangaru G, Suzuki K, Gillin MT, Mohan R, Titt U. An MCNPX Monte Carlo model of a discrete spot scanning proton beam therapy nozzle. Med. Phys. 2010; 37:4960–4970. [PubMed: 20964215]

Wang LLW, Perles LA, Archambault L, Sahoo N, Mirkovic D, Beddar S. Determination of the quenching correction factors for plastic scintillation detectors in therapeutic high-energy proton beams. Phys. Med. Biol. 2012; 57:7767–7782. [PubMed: 23128412]

Waters, LS.; Hendricks, J.; McKinney, G. Monte Carlo N-Particle Transport Code system for Multiparticle and High Energy Applications. Los Alamos, NM: Los Alamos National Laboratory; 2002.

Wilkens JJ, Oelfke U. Analytical linear energy transfer calculations for proton therapy. Med. Phys. 2002; 30:806–815. [PubMed: 12772988]

Wilkens JJ, Oelfke U. Three-dimensional LET calculations for treatment planning of proton therapy. Z Med Phys. 2004; 14:41–46. [PubMed: 15104009]

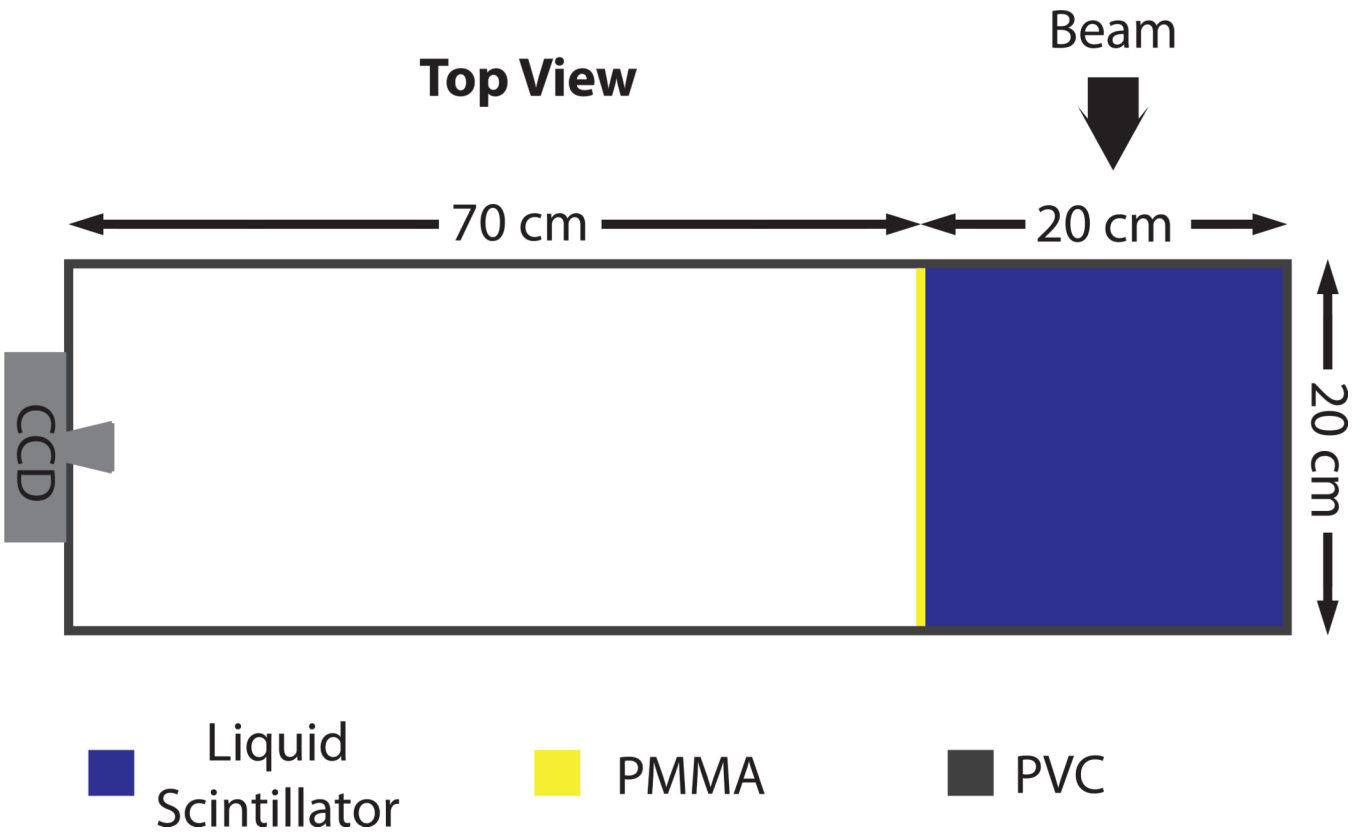

Figure 1.
Schematic of LS detector system.

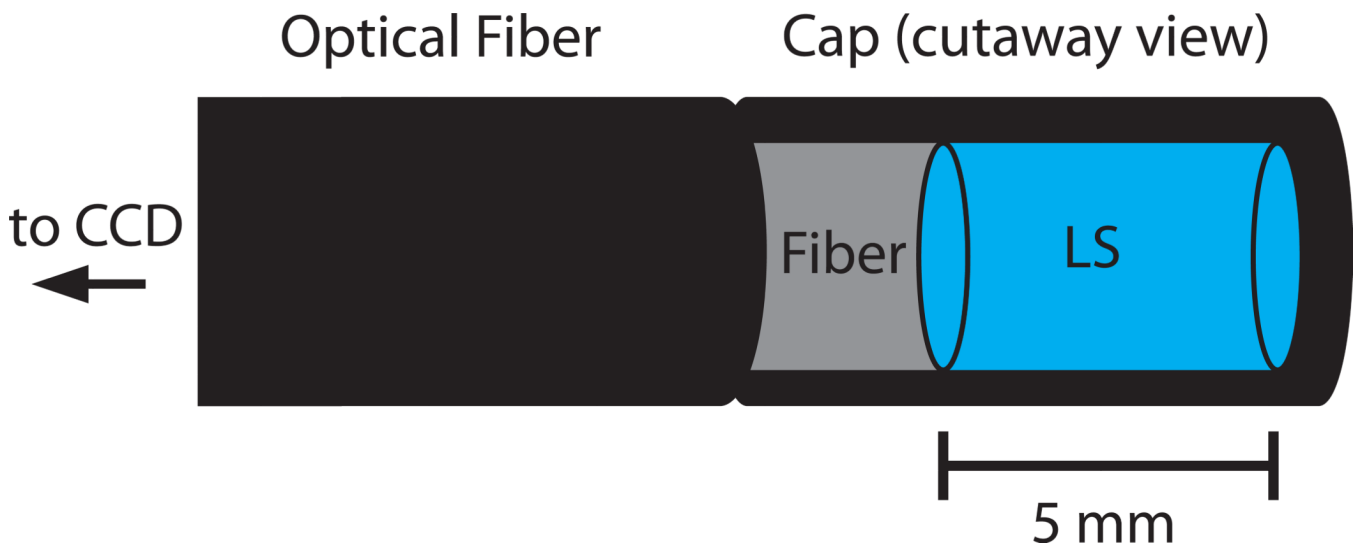

Figure 2.
Schematic of miniature LS detector.

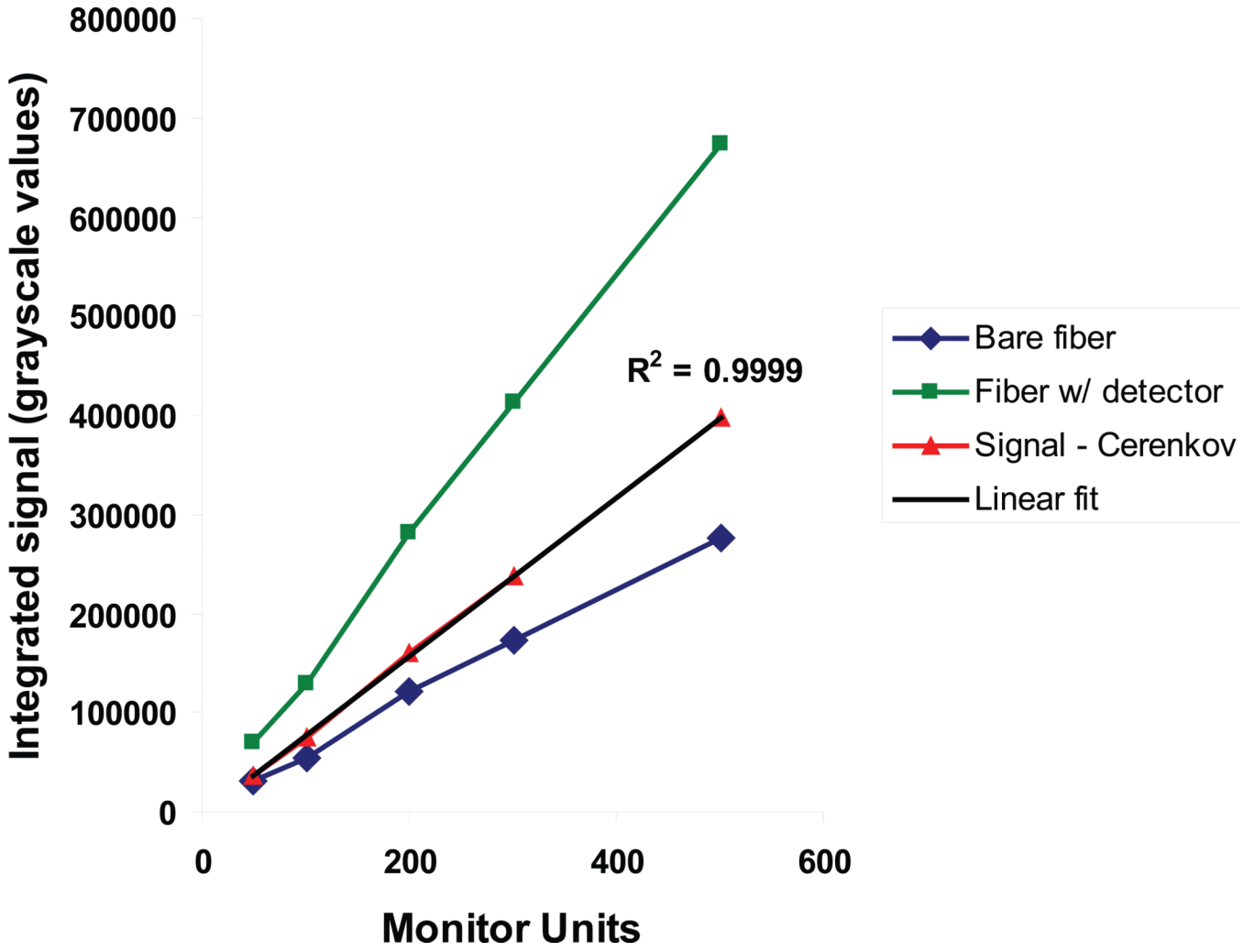

Figure 3.
The results of a linearity test of a miniature LS detector in a 6-MV photon beam. The scintillation light (red) was measured by subtracting the Cerenkov signal (blue) from the miniature LS detector signal (green). The R^2 value of a linear fit to the scintillation signal was 0.9999.

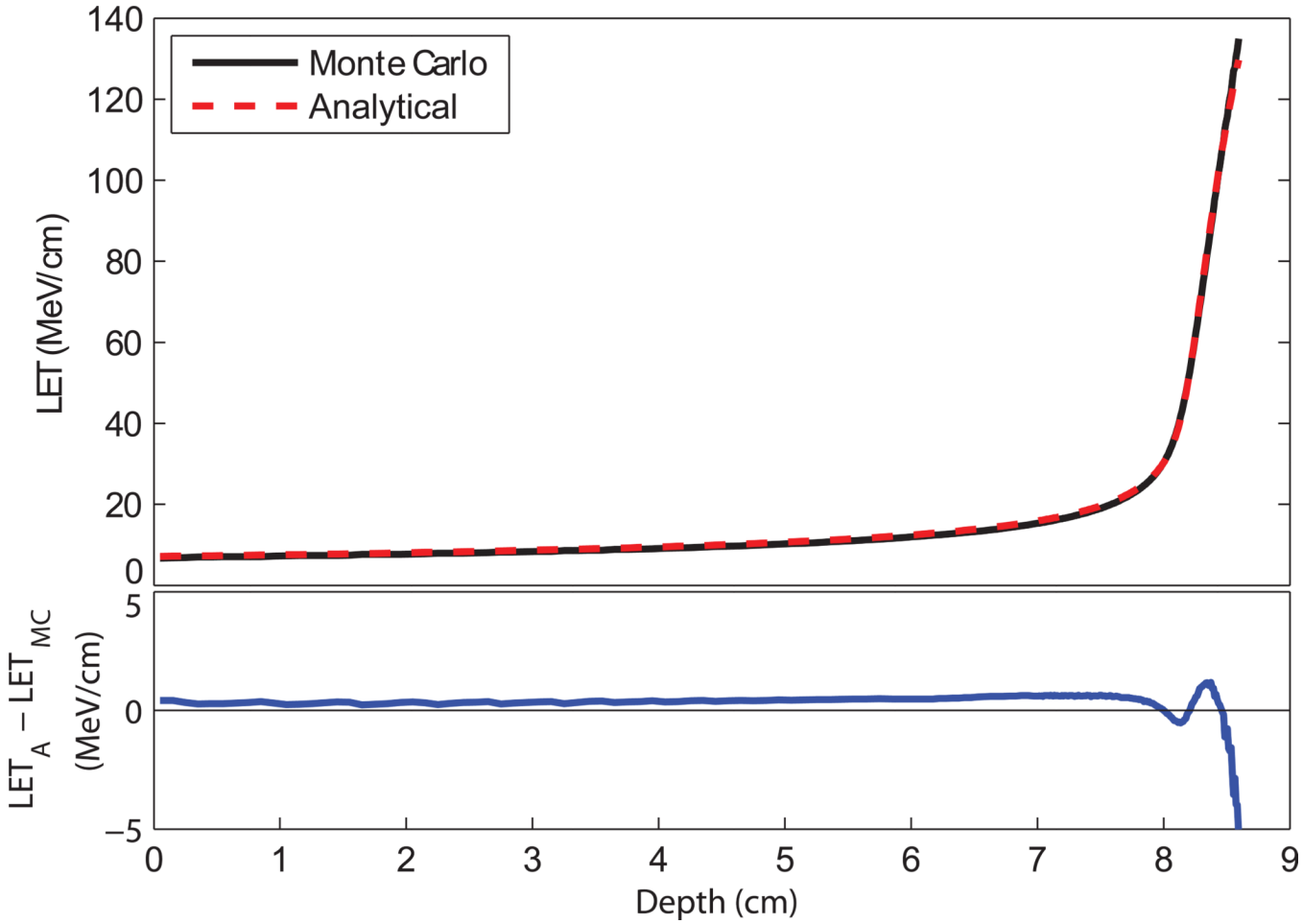

Figure 4.
(top) Track-averaged LET calculated with Monte Carlo methods and with an analytical formula for a 100.9-MeV proton beam in LS. (bottom) The difference between the analytically-derived LET values to the Monte Carlo-derived values.

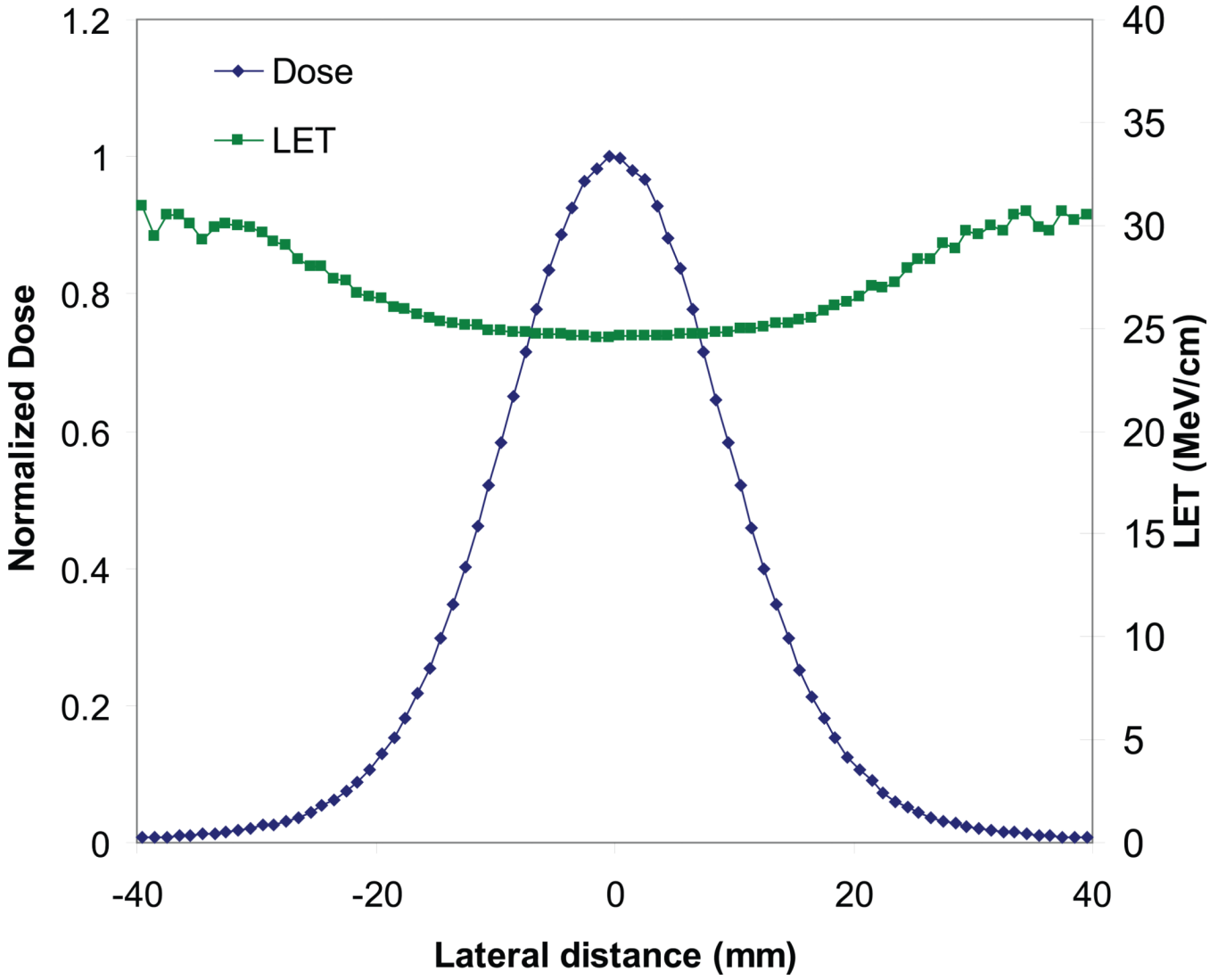

Figure 5.
The Monte Carlo LET calculation shows an off-axis LET increase of up to 22% in pixels containing 1% or more of the peak dose. The lateral dose profile is shown for reference.

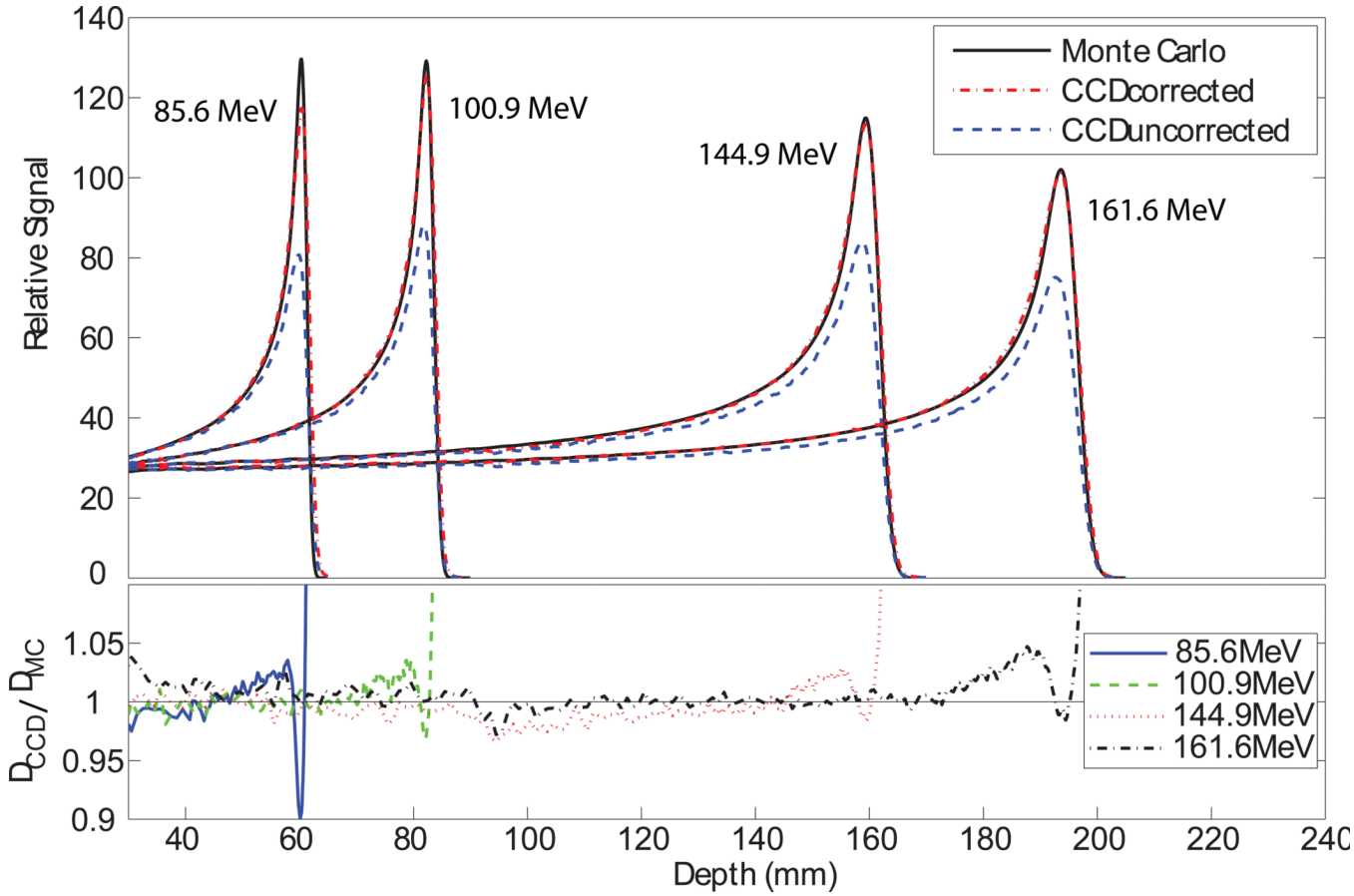

Figure 6.
(top) Central axis depth-dose profiles for proton pencil beams. The dose calculated by the validated Monte Carlo model is shown in black. The uncorrected scintillation signal is shown in blue. The corrected scintillation signal is shown in red. (bottom) The ratio of the corrected scintillation signal to the Monte Carlo dose.

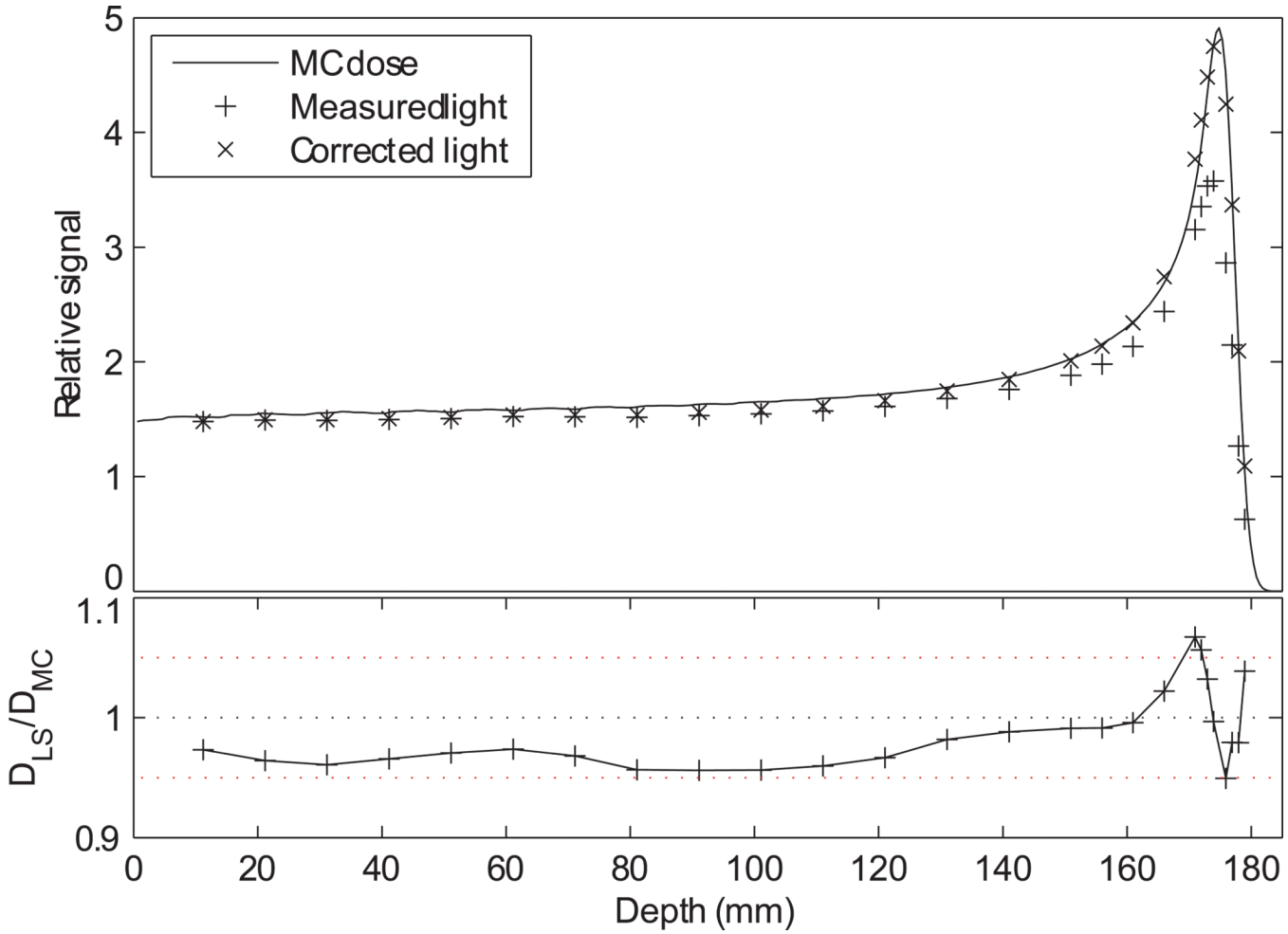

Figure 7.
(top) The light signal from the miniature LS detectors before (+) and after (x) the correction factor was applied. The dose from the Monte Carlo calculation is shown for comparison. (bottom) The ratio of the corrected light signal (D_{LS}) to the Monte Carlo dose (D_{MC}).

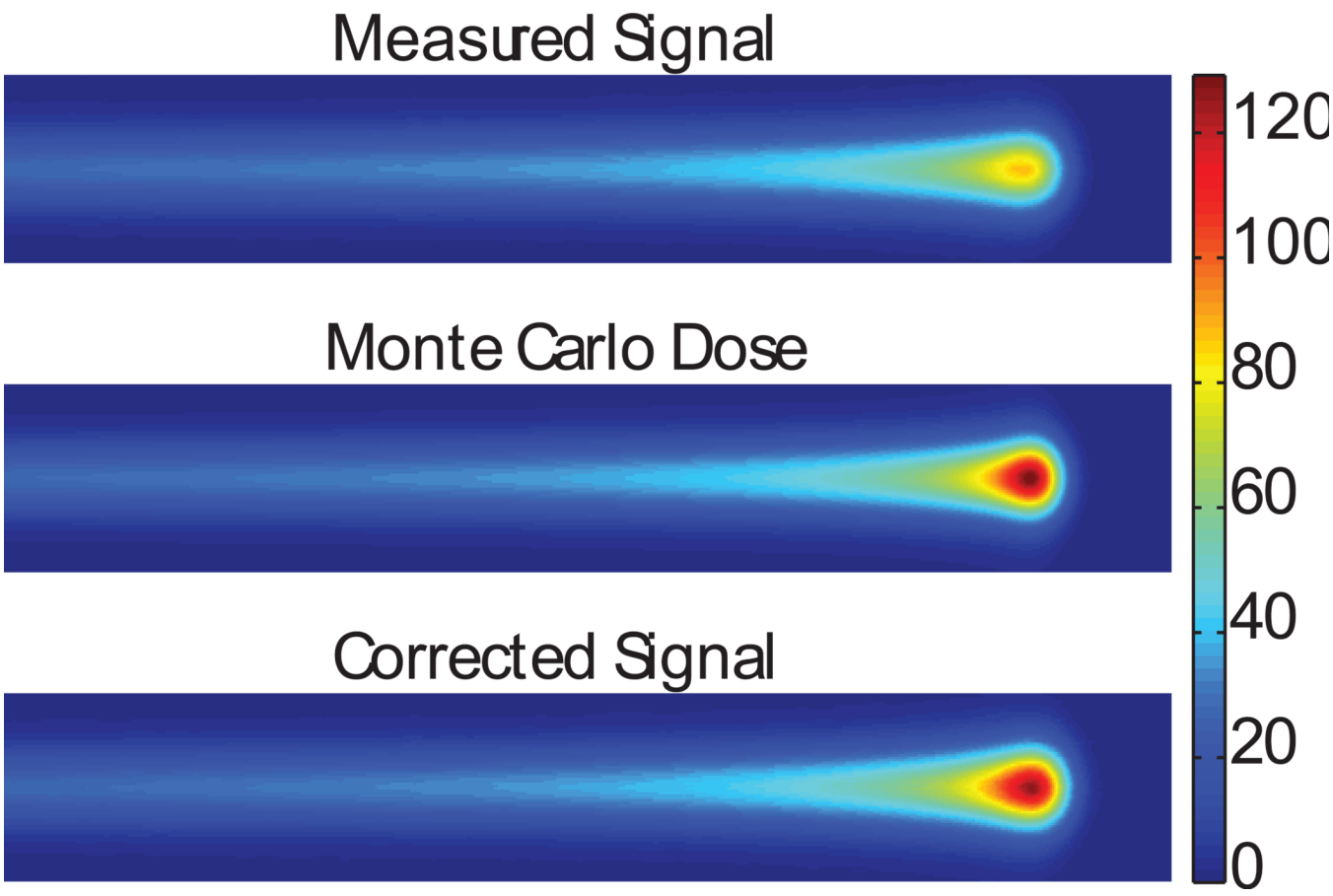

Figure 8.
The measured scintillation signal (top), the dose calculated using Monte Carlo methods (centre), and the corrected scintillation signal (bottom) for a 100.9-MeV proton pencil beam.

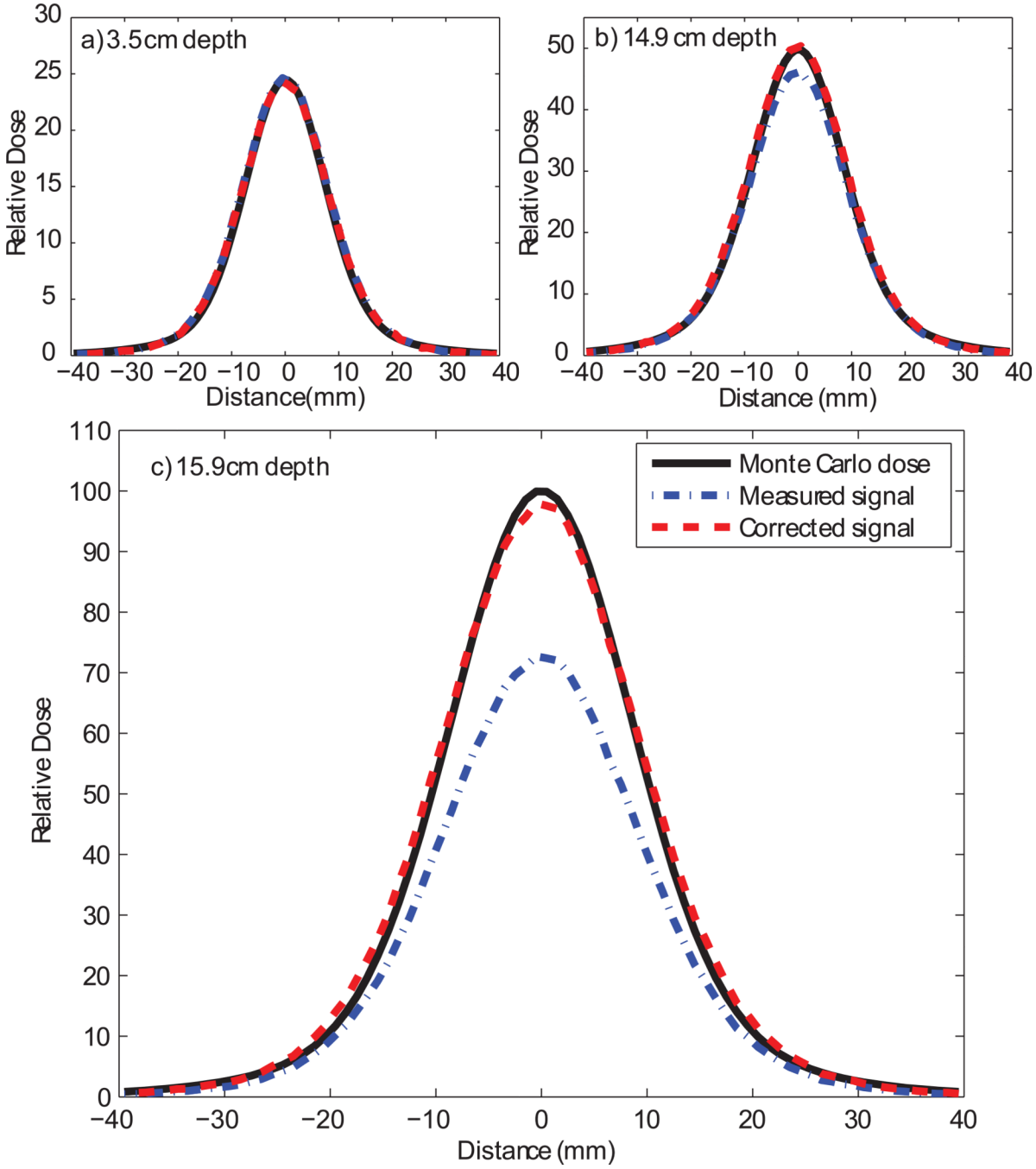

Figure 9.
Lateral dose profiles for a 144.9-MeV proton pencil beam at three depths: **a)** 3.5 cm (proximal build-up region), **b)** 14.9 cm (proximal 50% dose), and **c)** 15.9 cm (centre of Bragg peak).

Table 1

Peak-to-plateau ratios for the Monte Carlo dose calculation, the measured signal from the CCD, and the corrected CCD signal.

Energy (MeV)	Peak to Plateau Ratio		
	Monte Carlo	Measured Signal	Corrected Signal
85.6	4.04	2.51	3.70
100.9	4.40	3.01	4.30
144.9	4.09	2.99	4.10
161.6	3.78	2.78	3.69

Table 2

Percentage difference between the calculated peak height and the peak height from the measured and corrected CCD signals.

	Percent Difference from Monte Carlo	
Energy (MeV)	**Measured Signal (% difference)**	**Corrected Signal (% difference)**
85.6	37.7	9.5
100.9	31.8	2.6
144.9	26.9	1.5
161.6	26.4	0.7